



Enzymes Hot Paper

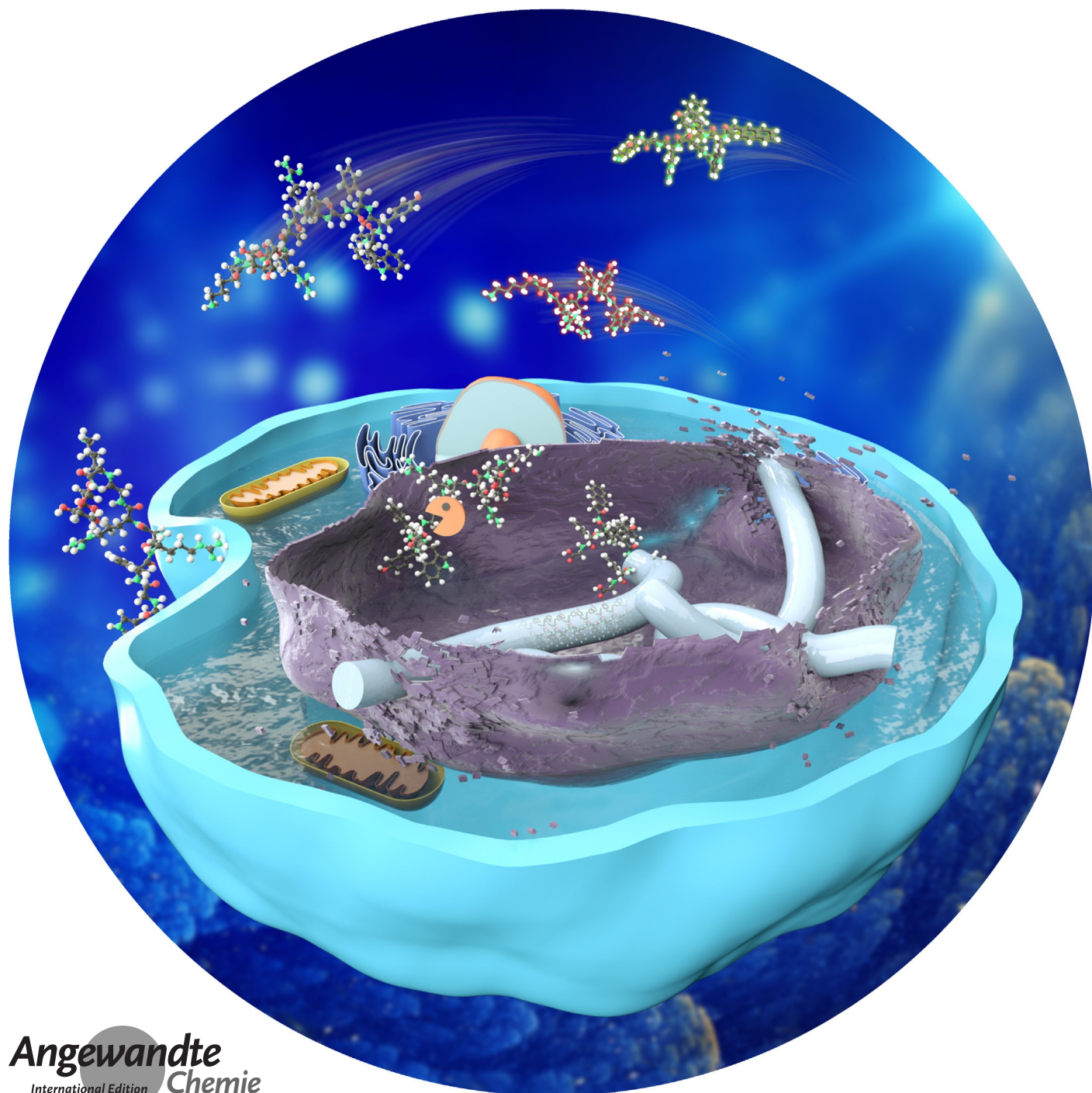
How to cite: *Angew. Chem. Int. Ed.* **2021**, *60*, 21807–21816

International Edition: doi.org/10.1002/anie.202103507

German Edition: doi.org/10.1002/ange.202103507

# Structure-Based Programming of Supramolecular Assemblies in Living Cells for Selective Cancer Cell Inhibition

Liangbo Hu, Ying Li, Xinhui Lin, Yucheng Huo, Hongyue Zhang, and Huaimin Wang\*

Angewandte  
International Edition  
Chemie

**Abstract:** Here we report on the design, synthesis, and assembly of an enzymatic programmable peptide system inspired by endocytic processes to induce molecular assemblies formation spatiotemporally in living cancer cells, resulting in glioblastoma cell death mainly in necroptosis. Our results indicate the stability and glycosylation of molecules play an essential role in determining the final bioactivity. Detailed mechanistic studies by CLSM, Flow cytometry, western blot, and Bio-EM suggest the site-specific formation of assemblies, which could induce the LMP and activate the downstream cell death pathway. Moreover, we also demonstrate that our strategy can boost the activity of commercial chemotherapy drug by escaping lysosome sequestration. We expected this work would be expanded towards artificial intelligent biomaterials for cancer therapy and imaging precisely.

## Introduction

Through non-covalent interactions, supramolecular self-assembly of synthetic objects is attracting substantial attention in recent years. Besides constructing functional materials in vitro for drug delivery, tissue engineering, regenerative medicine, analyte detection, immune modulation, and catalytic application, exploring functions of in situ formation of self-assembly structures in living cells have emerged as a promising frontier of supramolecular chemistry and materials science.<sup>[1]</sup> Biological relevant architectures formed by peptides have been extensively investigated in the past decades due to the ability of easily incorporating amino acid sequences, low immunogenicity, and ease of functionalization.<sup>[2]</sup> However, manipulating the higher-order assemblies formation of a synthetic molecule in living cell spatiotemporally with controllable function remains challenging because of a lack of suitable biocompatible stimulus and the complexity of the intracellular environment.<sup>[1c-e,2b,3]</sup>

To provoke the assembly of peptides into functional biomaterials (or higher-order assemblies) in the living cells, choosing a suitable stimulus is the key prerequisite for the function and location of the resulted assemblies. Among the several stimuli for triggering peptide self-assembly, enzyme instructed self-assembly (EISA) provides a unique opportunity to explore the formation of peptide assemblies for controlling cell behaviors in a complex cellular environment. Xu and co-workers reported the pioneering work that enzymatic formation of nanofibers of peptide amphiphiles in the pericellular space or inside cells, leads to selective cancer cell inhibition, minimized drug resistance, and 3D cell spheroid formation.<sup>[4]</sup> Ulijn et al. extended this concept using aromatic carbohydrate amphiphile as the simple building

block to generate a cytotoxic nanonet/hydrogel cage surrounding the cancer cells.<sup>[5]</sup> Besides using alkali phosphatase, Maruyama et al. employed a cancer-related enzyme (matrix metalloproteinase-7, MMP-7) to initiate intracellular self-assembly of a peptide lipid, leading to hydrogelation in cancer cells.<sup>[6]</sup> The success of these examples has stimulated the development of in situ forming higher-order structures for controlling cell behaviors and imaging.<sup>[7]</sup>

Despite the promises of using EISA for cancer therapy, achieving spatiotemporal control over the formation of assemblies with endogenous enzymes inside the cells is still challenging.<sup>[8]</sup> Moreover, most amphiphilic molecules usually have higher critical micellization concentration (CMC), resulting in suboptimal anti-cancer efficiency. Increasing the self-assembly ability of molecules with aromatic capping groups and organelle-selective accumulation of assemblies with targeting motifs are the efficient strategies to meet this challenge.<sup>[3b,9]</sup> However, the systematic study of the stability and the related activity of assemblies has yet to be explored. More importantly, EISA requires the precursor to meet the enzyme in the crowded environment or the confined compartments, thus limited its further application inside the cellular compartment.<sup>[10]</sup>

Inspired by the fact that most of the molecules access into cells through endocytosis, and cathepsin B (CTSB) are elevated in most solid tumors locating at the lysosome,<sup>[11]</sup> we hypothesize that CTSB could initiate molecular self-assembly after cellular uptake of the precursor, inducing cytotoxic assembly formation selectively in the confined environments of cancer cells, which could be a general method to induce assemblies formation selectively in live cancer cells. According to the substrate scope of CTSB, we rationally designed and synthesized a series of structural analogs of peptide precursors that differ in several key features: stereochemistry, C-terminal glycosylation, and regiochemistry. The results suggest that the expressing level of CTSB of different cells correlates very well with the bioactivity of molecular assemblies. We also show that the seral stability of the precursors has a significant impact on their final anti-cancer cell activity. Confocal laser scanning microscopy (CLSM) and biological electron microscopy (Bio-EM) imaging reveal the formation of intracellular assemblies in living cancer cells. Mechanistic studies by light scattering, CLSM, western blot, flow cytometry, and structure activity relationship (SAR) demonstrate that the precursors could be hydrolyzed by CTSB and self-assemble to form cytotoxic higher-order structures inside the lysosome, which further induction of lysosomal membrane permeabilization (LMP), resulting in glioblastoma cancer cell death selectively through necroptosis (Figure 1). Moreover, we also show that the intracellular formation of higher-order structures in lysosome could solve the challenge of drug sequestration toward cancer cells.

## Results and Discussion

Figure 2 shows the molecular design of the representative structures of the precursors for CTSB instructed self-assembly.

[\*] Dr. L. Hu, Y. Li, X. Lin, Y. Huo, H. Zhang, Prof. H. Wang  
Key Laboratory of Precise Synthesis of Functional Molecules of Zhejiang Province, School of Science, Westlake University, Institute of Natural Sciences, Westlake Institute for Advanced Study  
18 Shilongshan Road, Hangzhou 310024, Zhejiang Province (China)  
E-mail: wanghuairmin@westlake.edu.cn

Supporting information and the ORCID identification number(s) for the author(s) of this article can be found under:  
<https://doi.org/10.1002/anie.202103507>.

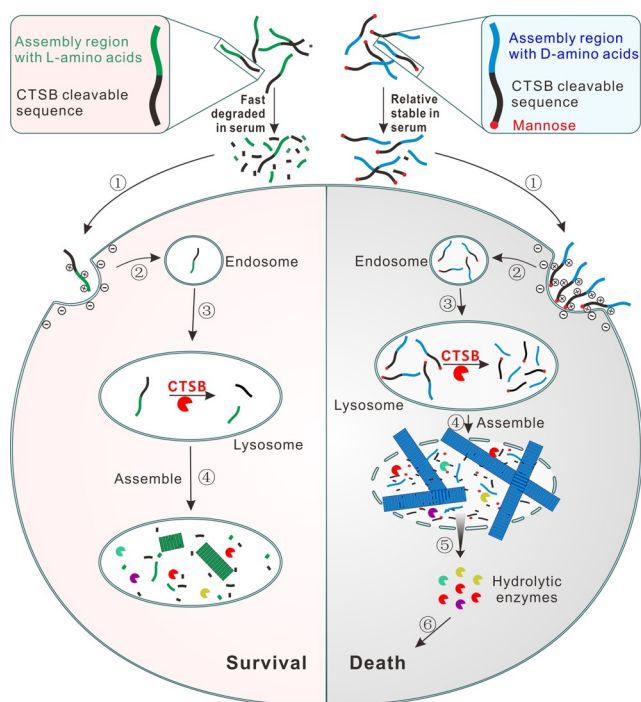
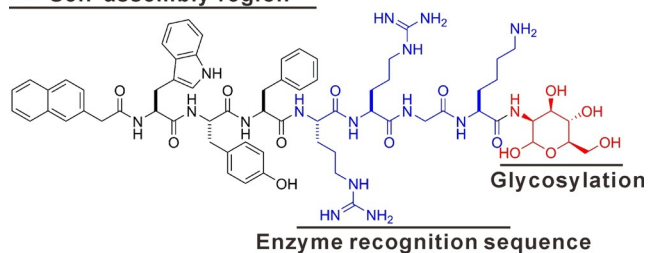


**Figure 1.** Representation of the formation of functional higher-order assemblies in living cells for selective cancer cell inhibition.

### A Self-assembly region



### B

Peptide	Sequence
<b>L-N</b>	Nap-WYFRRGK
<b>L-NM</b>	Nap-WYFRRGK-Man
<b>D-N</b>	Nap-wyfrgk
<b>D-NM</b>	Nap-wyfrgk-Man
<b>DL-N</b>	Nap-wyfRRGK
<b>DL-NM</b>	Nap-wyfRRGK-Man
<b>DL-NA</b>	Nap-wyfGFRARGK
<b>DL-NAM</b>	Nap-wyfGFRARGK-Man

**Figure 2.** A) Illustration, and B) sequences of CTSB responsible self-assembly peptides (molecular structures are in Scheme S2). Nap, naphthylacetic acid; Man, Mannosamine.

bly. The molecules consist of the following four distinct parts: i) the naphthyl group to enhance the self-assembly in living cell by providing strong aromatic-aromatic interaction;<sup>[12]</sup> ii) tripeptide of Trp-Tyr-Phe (WYF) serves as a self-assembling backbone by providing  $\pi$ - $\pi$  interaction and hydrogen bonding; iii) peptide sequence Arg-Arg-Gly-Lys (RRGK) provides the hydrophilic part and serves as the enzymatic cleavage site for CTSB;<sup>[13]</sup> iv) C-terminal glycosylation, a common post-translational modification of the protein, increases the stability of molecules in the serum and inside

cells.<sup>[14]</sup> Based on the above design, we also set out to synthesize the non-cleavage peptides **D-N** and **D-NM** (Figure 2B) consisting of D-amino acids as the control. The difference in the stereochemistry of the self-assembly motif (L-WYF and D-wyf) would verify whether the stability of molecules contributes to the bioactivities of the assemblies. To decrease the precursor's CMC, we also used Gly-Phe-Arg-Ala-Arg (GFRAR) to replace RR because the latter is more hydrophilic at lysosomal acidic environment due to protonation. The designed molecules and the corresponding self-assembling molecules are accessible through a facile synthetic procedure (Supporting Information, Scheme S1). All the peptides were synthesized using standard Fmoc based solid-phase peptide synthesis (SPPS) and purified by preparative high-performance liquid chromatography (HPLC). We obtained glycosylated peptides by directly coupling the carboxylic acid with mannosamine after purification by HPLC. We used liquid chromatography-mass spectrometry (LC-MS) and HR-MS (Figures S1–S3 and Table S3) to confirm the structures of the molecules after HPLC purification.

To demonstrate the concept of CTSB instructed cellular self-assembly for selectively killing cancer cells that expressing certain levels of CTSB, we first measured the expression levels of CTSB in four cell lines, including two cancer cell lines of HeLa and U87MG, and two non-cancer cell lines of HS-5 and MCF-10A. According to western blot analysis, HeLa and U87MG cell lines express almost the same level of CTSB, which are higher than HS-5 and MCF-10A cell lines (Figure 3A and B). The relative CTSB expression level of U87MG cells is about 1.5 times higher than that of HS-5 cells (or MCF-10A cells). To confirm our assumption, we next treated these cell lines with the above precursors to evaluate their cytotoxicity (Figure 3C and S4–7). The results show that all the precursors exhibit the lowest  $IC_{50}$  against U87MG cells than other cell lines except **DL-NA**. The  $IC_{50}$  value of **L-N**, **L-NM**, **DL-N**, **DL-NM**, and **DL-NAM** against U87MG cells is 143.2, 58.7, 59.3, 59.2, and 38.5  $\mu$ M, respectively. The  $IC_{50}$  value of these precursors against two normal cells of HS-5 cells and MCF-10A cells is more than two times greater than against U87MG cells (Figure 3C and Table S4), which is consistent with the expression level of CTSB. The  $IC_{50}$  of these precursors against HeLa cells follows the trend of **DL-NAM** (35.2  $\mu$ M) < **DL-NM** (66.5  $\mu$ M) < **DL-NA** (92.9  $\mu$ M) < **L-NM** (198.5  $\mu$ M) = **DL-N** (198.5  $\mu$ M) < **L-N** (> 500  $\mu$ M). More interestingly, we also found that stereochemistry and glycosylation of peptide could influence the anti-cancer cell efficiency of the peptide. Specifically, all glycopeptides exhibit lower  $IC_{50}$  than the corresponding peptides without glycosylation, suggesting that the stability of EISA precursor could play a key role in determining the final anti-cancer cell activity.

The stability represents an important characteristic for the activity of EISA precursor. However, the systematic study of the stability of precursor in serum has yet to be explored in using EISA to kill cancer cells.<sup>[1b,c,4c]</sup> The serum contains a wide variety of proteinases and peptidases, affecting the final anti-cancer cell efficacy of self-assembling peptides. Thus, we next investigate the stability of EISA precursor in minimal essential medium (MEM) supplemented with 10%

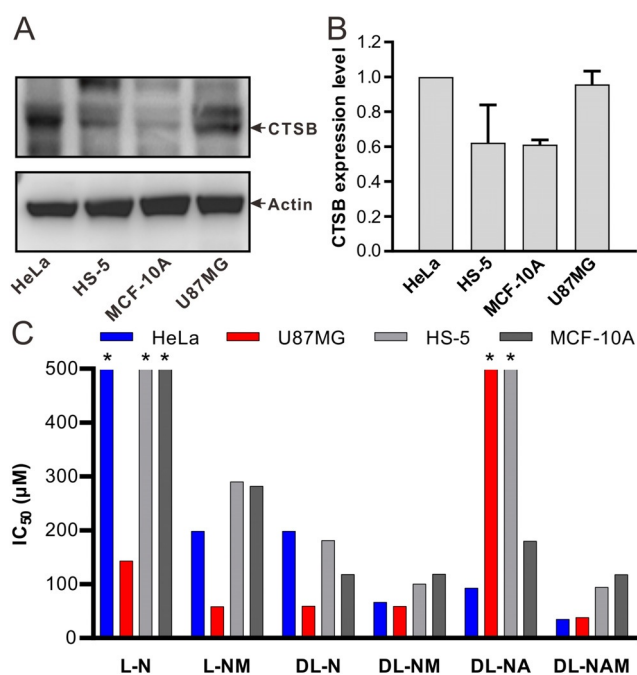


**Figure 3.** A) CTSB expression levels in cancer cells (HeLa and U87MG) and non-cancer cells (HS-5 and MCF-10A) that detected by western blot. B) Quantification of CTSB expression levels from (A). The gray values of CTSB were divided by that of actin. All data are normalized to HeLa cells (set as 1). C) IC<sub>50</sub> of EISA precursors in HeLa, U87MG, HS-5 and MCF-10A. \*, > 500 μM.

fetal bovine serum (FBS). The results show that glycopeptides are more stable than the corresponding original peptides. The degradation ratio (Figure 4 A and Figure S8) of all the EISA precursors follows the trend of **DL-NA** (98.7%) > **L-N** (98.1%) > **DL-N** (93.2%) > **DL-NAM** (50.6%) > **L-NM** (37.4%) > **DL-NM** (26.1%), agreeing with the reported work that using glycosylation of peptide to improve the stability of biomaterials forming by peptides.<sup>[14,15]</sup> Concentration-dependent degradation experiments (Figure S9) suggest that the glycosylated peptide are more stable in aggregation state, while the non-glycosylated peptides exhibit almost the similar degradation behavior in molecularly dissolved species, or as fibrous aggregates, implying that glycosylated peptides could circulate as fibrous aggregates in cell level. To investigate the self-assembly properties of the EISA precursors, we further verified that CTSB was able to convert the precursor to a corresponding self-assembling molecule, which then self-assemble into higher-order structures. We used LC-MS to quantify the cleavage ratio of EISA precursors (Figure 4B, Figure S10 and Table S5) after addition of CTSB (5 U mL<sup>-1</sup>). After 24 h incubation, the percentages of the enzymatic product of **L-N** and **L-NM** are about 93.0% and 67.9%, while the conversion percentages of **DL-N**, **DL-NM** are about 42.6% and 54.5%, indicating the stereochemistry could affect the enzymatic rate of EISA precursor. We also found that **DL-NAM**, the most hydrophobic precursor, exhibits slower molecular transformation, which is about 36.7%, suggesting the balance of hydrophobic and hydrophilic parts in the precursor could influence the EISA kinetics.<sup>[16]</sup> We also investigate the enzymatic conversion of precursors at the

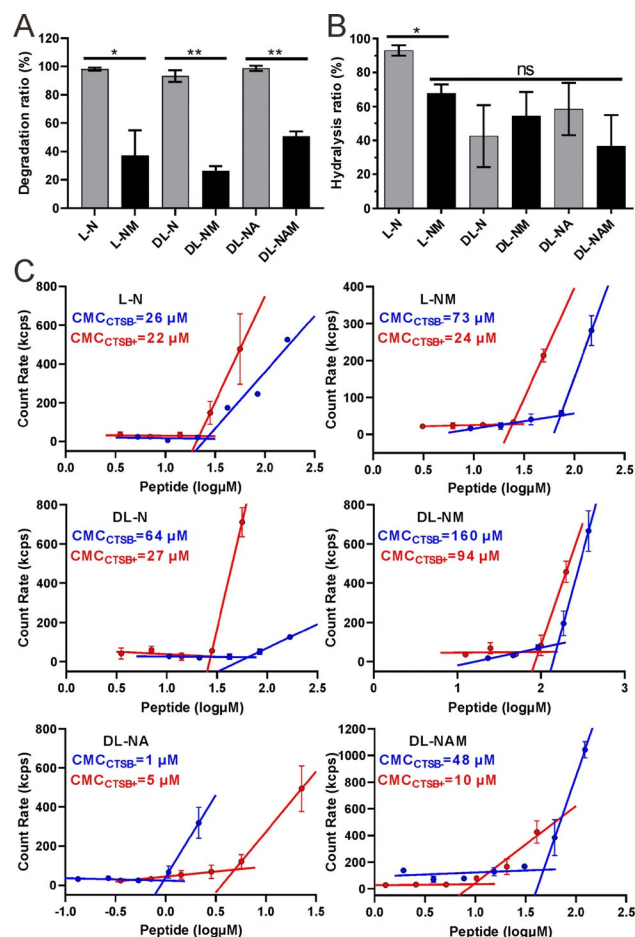


**Figure 4.** A) Degradation ratio of peptides incubated in MEM supplemented with 10% FBS at 37°C for 2 h. The concentration of peptides is 100 μM. B) Hydrolysis ratio of peptides that treated with CTSB. 0.2 mg mL<sup>-1</sup> peptides were incubated with 5 U mL<sup>-1</sup> CTSB at 37°C for 24 h before being quantified by LC/MS. Student's t test was performed: \*,  $P < 0.05$ ; \*\*,  $P < 0.01$ ; ns, no significance. C) CMC of peptides. Peptides were incubated with (CTSB+) or without (CTSB-) 5 U mL<sup>-1</sup> CTSB at pH 6.0 for 24 h and then detected by dynamic light scattering (DLS) for CMC calculation.

concentration of 25 μM and 100 μM, the results (Figure S11) indicate that the aggregation of the precursors slightly influences their enzymatic conversion ratio. Compared the CMC values with enzymatic conversion of precursors, our results also suggest that the enzymatic reactivity is not related to the solubility (all peptides are dissolved very well in aqueous solution) or CMC values of precursors. Hydrolysis experiments also show that **D-N** and **D-NM** hardly be cleaved by CTSB (Figure S12), agreeing with their low bioactivity towards cancer cells (Figure S13).

To investigate the influence of physicochemical properties of assemblies on their bioactivities, we first assess the critical micellization concentration (CMC) of EISA precursors before and after addition of CTSB by dynamic light scattering. The results (Figure 4C) indicate that C-terminal modification of peptide with mannose decreases the self-assembly ability of the precursors, as evidenced by the CMC values, which follows the order of **DL-NA** (1 μM) < **L-N** (26 μM) <

**DL-NAM** (48  $\mu\text{M}$ ) < **DL-N** (64  $\mu\text{M}$ ) < **L-NM** (73  $\mu\text{M}$ ) < **DL-NM** (160  $\mu\text{M}$ ). Although enzymatic hydrolysis of the glycosylated peptides and the non-glycosylated peptides should yield the same peptide, the hydrolysis rate and the final hydrolysis percentage of glycosylated and non-glycosylated peptides could also influence the final CMC values of molecules after hydrolysis by enzymes. Compared to the corresponding precursors, the CMC values of assemblies formed by EISA decreased by 1.2 (**L-N**), 1.7 (**DL-NM**), 2.4 (**DL-N**), 3.0 (**L-NM**), and 4.9-fold (**DL-NAM**), respectively, with **DL-NA** as an exception, of which CMC increased 5.1 times. Zeta potential measurements (Figure S14) show that all the precursors at concentration near or higher than CMC have positive charges, suggesting the positively charged aggregate state of precursors could contribute to their interaction with negatively charged cancer cell membranes.<sup>[17]</sup> Together with the bioactivity and stability of precursors, these results suggest the complexity of in situ formation of assemblies in living cells, and elucidating the exact contributions of each factor will advance these fields.

We then studied the morphologies of EISA precursors before and after the addition of CTSB by cryogenic electron microscopy (cryo-EM). The results show that before adding enzymes, the precursors (excluding **DL-NM**) form uniform nanofibers at the concentration near the  $\text{IC}_{50}$ , which have subtle changes after the addition of CTSB (Figure 5). **DL-NM** form few amorphous aggregates before the addition of CTSB, which transform into unique nanofibers with a diameter of 5.9 nm in several micrometer length. Additionally, **DL-N**, **DL-NM**, **DL-NAM** did not form nanofibers at 25  $\mu\text{M}$  (lower than CMC of most peptides except **DL-NA**), but transformed to nanofibers after addition of CTSB (Figure S15). Circular dichroism (CD) experiments also reveal a subtle difference between EISA precursor and the assemblies after the addition of CTSB (Figure S16). Together, these results suggest that the aggregates rather than the monomers of EISA precursor are the first step in determining the anti-cancer cell activity.

To directly visualize the cellular distribution and the dynamic properties of assemblies formation in living cells, we designed and synthesized six fluorescent EISA precursors by replacing the naphthyl group with a fluorophore nitrobenzoxadiazole (NBD) at the N-terminal of peptides, resulting in **fL-N**, **fL-NM**, **fDL-N**, **fDL-NM**, **fDL-NA**, **fDL-NAM** (Scheme S2). The fluorescent analogs show similar self-assembly properties and bioactivities with their original Nap-precursors (Figures S17–S19). The CLSM results reveal that most of the green fluorescence from assemblies of peptides co-localize with red fluorescent dots from LysoTracker in U87MG cells at 2 h (Figure 6A). After 24 h incubation, almost all the green fluorescent dots co-localize with the red fluorescent dots from LysoTracker, suggesting the uptake of peptides by cells via endocytosis and accumulate in lysosomes with the increase of time. We next used flow cytometry to quantify the assemblies within cells after 2 and 24 h incubation. The results indicate that the cellular uptake of **fDL-NM** and **fDL-NAM** is higher than **fDL-N** and **fDL-NA** at 24 h, which is about 1.1 and 1.9 fold, respectively (Figure 6B and C). Compared with the uptake of **fL-N** (**fL-**

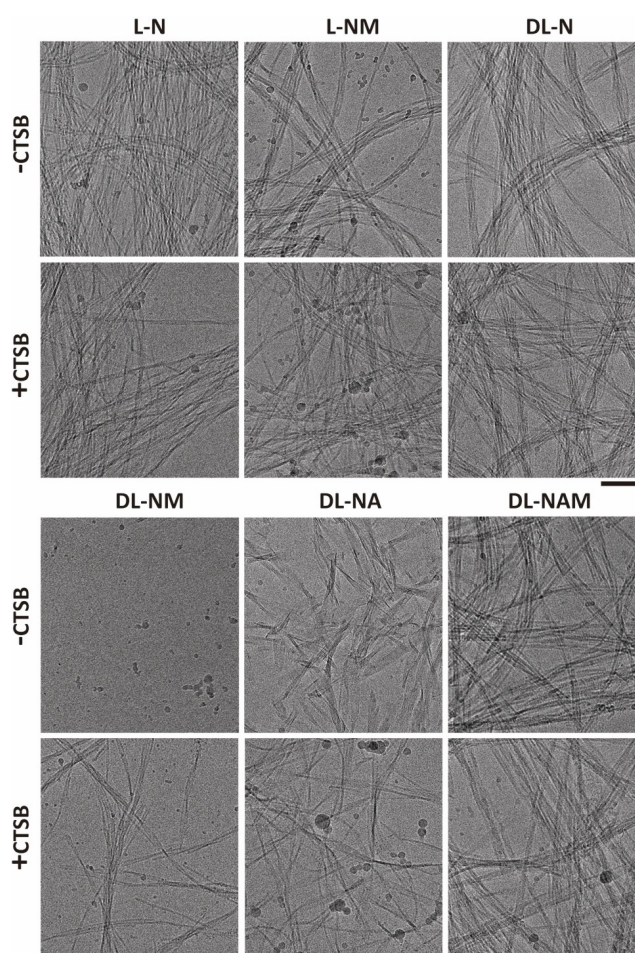


**Figure 5.** Cryo-EM images of nanostructure formed by **L-N**, **L-NM**, **DL-N**, **DL-NM**, **DL-NA**, and **DL-NAM** before and after the addition of CTSB (5  $\text{U mL}^{-1}$ ). The concentration of all the molecules is 0.2  $\text{mg mL}^{-1}$ . Scale bar: 100 nm.

**NM**), cellular uptake of **fDL-N**, **fDL-NM**, **fDL-NA**, and **fDL-NAM** shows 6.5, 7.1, 3.0 and 6.0 fold increase in fluorescence intensity, respectively, indicating the stability of peptides could affect the accumulation of peptides in living cells. Concentration-dependent studies suggest that the maximum fluorescent intensity of cells is achieved at 24 h (50  $\mu\text{M}$ ) and 6 h (100 or 150  $\mu\text{M}$ ), respectively (Figure S20). At 1 h, the fluorescent intensity of cells treated with 100  $\mu\text{M}$  of **fDL-NAM** is about two fold of the cells treated with 50  $\mu\text{M}$  of **fDL-NAM**, while the fluorescent intensity of cells treated with 150  $\mu\text{M}$  of **fDL-NAM** is about 3.5 fold of cells treated with 100  $\mu\text{M}$  of **fDL-NAM**. These results suggest that the aggregation state of peptide could promote the cellular uptake of molecules.

To investigate the dynamic self-assembly process of precursor and their interaction with the plasma membrane in living cells, we obtained living cell video (Video clip S1) of U87MG cells. The results show that the precursor **fDL-NAM** binds to the cell surface quickly (in 1 minute) and show puncta fluorescence in the endosomes through endocytosis (Figure S21). We also examine the precursors' membrane-binding capability by incubating cells on ice and measuring

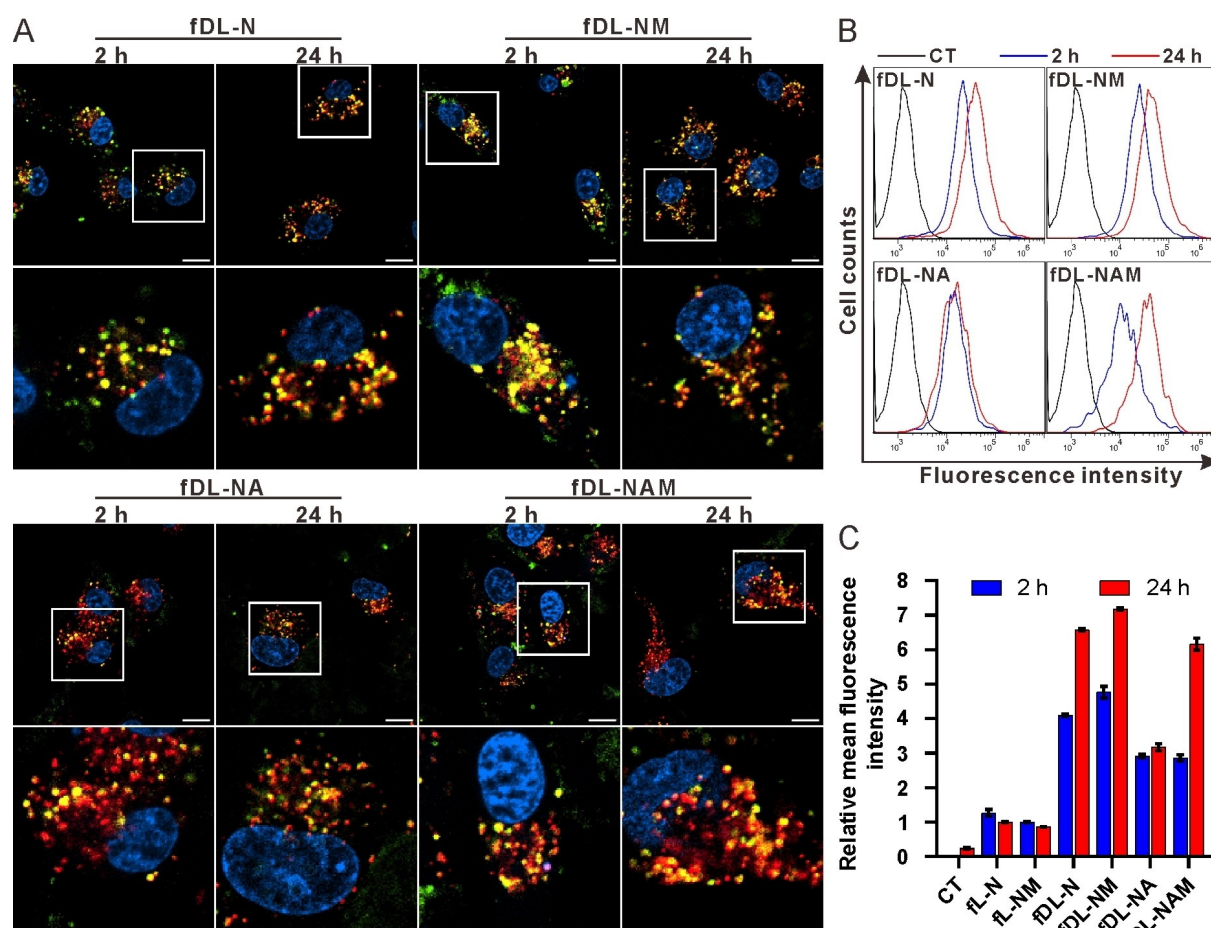


**Figure 6.** A) Subcellular distribution of NBD labelled peptides. U87MG cells were incubated with 62.5  $\mu\text{M}$  peptides (Green) for 2 or 24 h before being stained by LysoTracker Deep Red (Red) and imaged by CLSM. Scale bar: 10  $\mu\text{m}$ . B) Histogram of flow cytometry. U87MG cells incubated with 62.5  $\mu\text{M}$  NBD labelled peptides for 2 or 24 h, and then detected by flow cytometry. C) Mean fluorescence intensity of flow cytometry. The data are normalized to that of fL-N at 24 h (set as 1).

NBD's fluorescence intensity by a microplate reader. Glycopeptides bind equally to the corresponding ones without mannose in HeLa cells, except fL-NM (Figure S22). The binding ability of EISA precursors with cell membrane follows the order of fDL-NA (fDL-NAM) > fL-N > fL-NM = fD-N (fD-NM) > fDL-N (fDL-NM). In U87MG cells, only fDL-NM binds U87MG cells slightly higher than fDL-N, while fL-NM and fDL-NAM bind lower than fL-N and fDL-NA, respectively. These results, together with the zeta potential properties of the precursor, suggesting the interactions between the precursors and cell membrane are the important step for their further bioactivity.

To investigate the essential role of CTSB for bioactivity of assemblies, we co-incubate a CTSB specific inhibitor CA-074Me<sup>[18]</sup> with precursor during cell viability experiment. Co-incubating the inhibitor CA-074Me significantly reduced the cytotoxicity of five EISA precursors (L-NM, DL-N, DL-NM, DL-NA, and DL-NAM) in HeLa and four (L-NM, DL-NM, DL-NA, and DL-NAM) in U87MG cells (Figures S23, S24), indicating the vital process of EISA in anti-cancer cell efficiency. After being endocytosed and transferred to lysosomes, CTSB in the lysosome could convert the EISA precursors to the corresponding self-assembly molecules,

which further self-assembly to form functional structures in the lysosome and lead to lysosome membrane permeabilization (LMP). To test this hypothesis, we used acridine orange (AO)<sup>[19]</sup> to stain HeLa (Figure S25) and U87MG cells (Figure 7A) before and after incubating with the cytotoxic precursor DL-NAM, respectively. Generally, AO emits green fluorescence. Once it accumulates and aggregates in the acidic lysosome, AO also emits red fluorescence. We observed dot-shaped red fluorescence and diffusive green fluorescence accompanying some aggregates in the control group. After the addition of DL-NAM (250  $\mu\text{M}$ ) for 2 h, the dot-shaped red fluorescence transferred to diffusive fluorescence in some cells, while the red fluorescence is diffusive in almost all cells at the concentration of 500  $\mu\text{M}$  (2 h), indicating the occurrence of LMP. We also used another dye, Magic Red (MR), to further confirm LMP induced by assemblies. MR shows no fluorescence and will emit red fluorescence after hydrolyzation by CTSB.<sup>[20]</sup> Thus MR can indicate the distribution of CTSB and the integrity of lysosome where CTSB is mainly located. The dot-shaped fluorescence of MR in normal cells without treatment is consistent with the distribution of CTSB in lysosomes (Figure 7B). After the addition of DL-NAM, the dot-shaped fluorescence of MR becomes diffusive,

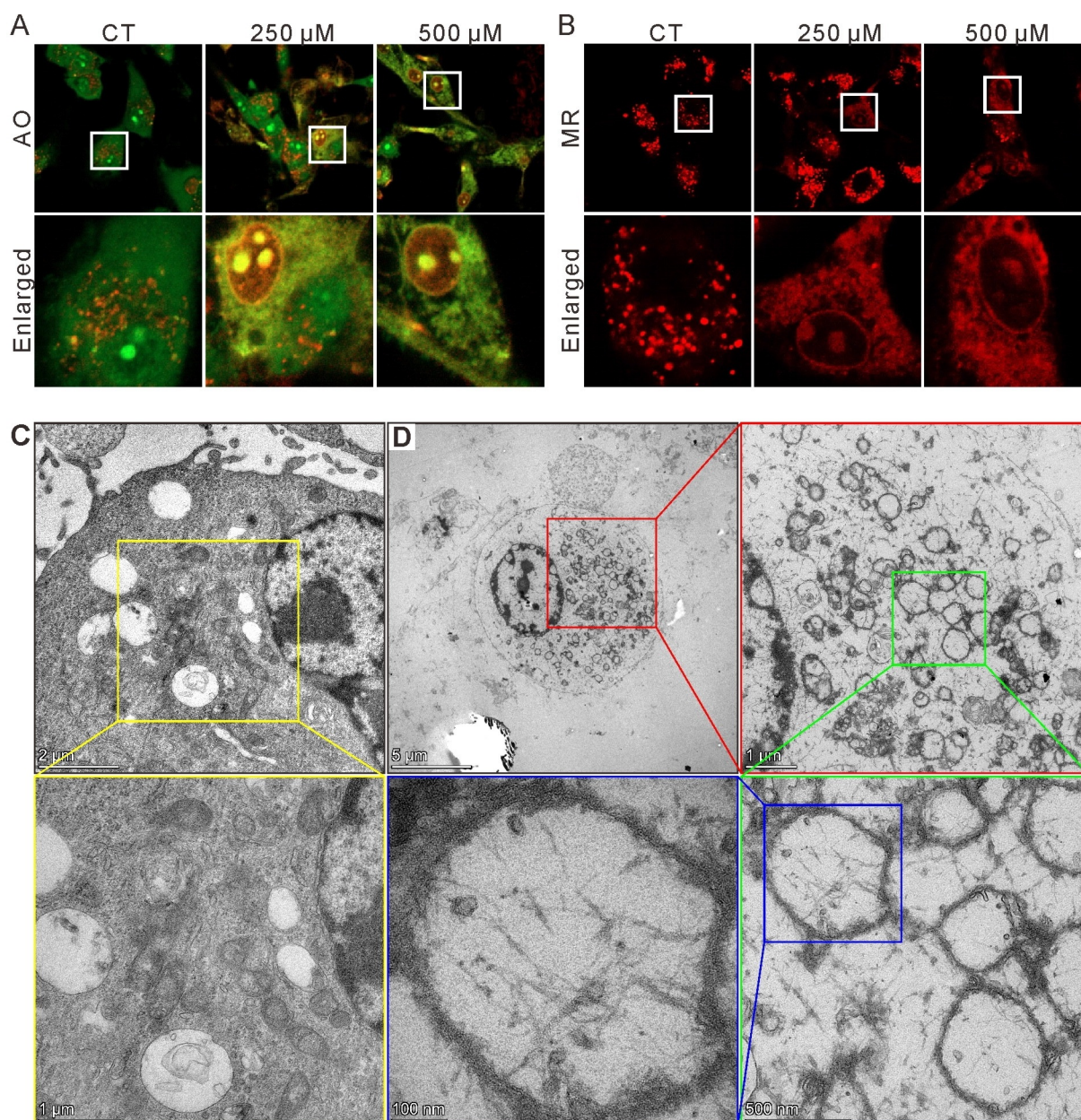


**Figure 7.** A) U87MG cells were incubated with 250 or 500  $\mu\text{M}$  DL-NAM for 2 h, and stained with AO. Fluorescence images were captured at excitation = 488 nm/emission = 510–550 nm (Green), and excitation = 561 nm/emission = 610–700 nm (Red). B) U87MG cells were incubated with 250 or 500  $\mu\text{M}$  DL-NAM for 1 h and incubated for another 1 h with addition of MR. Fluorescence images were captured at excitation = 561 nm/emission = 610–700 nm (Red). C) Bio-EM images of U87MG cells incubated without peptide. D) U87MG cells incubated with 200  $\mu\text{M}$  DL-NAM for 24 h.

indicating CTSB released from disrupted lysosomes to the cytosol. To visualize the morphology change of lysosome and in situ assembly of EISA precursors, we used Bio-EM to detect the U87MG cells after incubating with EISA precursors (L-N, L-NM, DL-NM, and DL-NAM). Compared to the control cells (Figure 7C), the cells treated with DL-NAM (Figure 7D) and DL-NM (Figure S26) exhibit distinctive nanofibers inside and outside lysosomes. The morphology of intracellular nanofibers is similar to the in vitro experiments by TEM. We also found that cells treated with DL-NAM and DL-NM have almost no integral organelles except many large vacuoles containing nanofibers. L-NM treated cells were also

vacuolated, but we could only observe nanofibers existing in few cells (Figure S26). Cells incubated with less toxic L-N show similar morphology to the control group (Figure S26). These in situ assembly is due to the enzymatic transform of EISA molecules as inhibitor of CTSB could block it (Figure S27). These results demonstrate that the designed EISA molecules can assemble in cancer cells and lead to cell vacuolization, resulting in cell death selectively.

To explore the cell death mechanism induced by assemblies, we detected the apoptosis and necroptosis of U87MG cells treated with DL-NAM by staining cells with YO-PRO-1 (Y1, for apoptosis) and propidium iodide (PI, for necrosis)

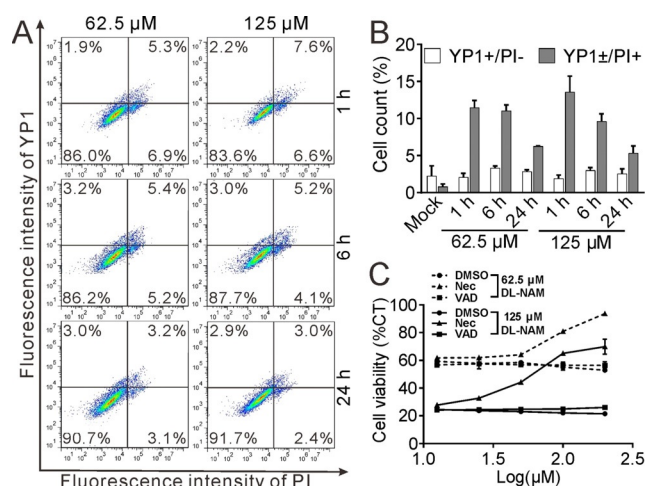


**Figure 8.** A) Plot graph of U87MG cells stained by PI and YP1. B) Percentage of apoptosis (YP1 +/PI−) and necrosis (YP1 ±/PI+) cells. C) Cell viability of U87MG incubated with DL-NAM and Necrostatin-1 (Nec) or Z-VAD-fmk (VAD).

(Figure 8A and B). The results indicate that there is no significant difference of apoptosis (YP1 +/PI−) between the control group and DL-NAM treated cells, while necrosis (YP1 ±/PI+) increased up to 17-fold at 1 h later after treated with DL-NAM (125 μM). The necrosis ratio decreased from 1 h to 24 h when cells were treated by DL-NAM (62.5 μM or 125 μM). A possible reason for this is that necroptotic cells became unstainable with the increase of incubation time. We observed the highest necroptosis ratio of U87MG cells treated by 62.5 or 125 μM DL-NAM at 1 h, indicating the DL-NAM induced necroptosis is fast and may cover up the sluggish apoptosis. Western blot experiments also show moderate apoptosis is induced by DL-NAM (Figure S28). Furthermore, the cytotoxicity of DL-NAM was slightly reduced when U87MG cells co-incubated with DL-NAM and an apoptosis specific inhibitor of Z-VAD-FMK (VAD) (Figure 8C), indicating apoptosis only plays a minor role in EISA induced cell inhibition. In contrast, co-incubation with DL-NAM (62.5 or 125 μM, 24 h) and an inhibitor of necrosis (Necrostatin-1, Nec) rescued the cell viability from 60 % to 90 % or from 25 % to 65 %, respectively, demonstrating necroptosis plays the major role in EISA induced cell inhibition. Inhibition of CTSB could reduce the toxicity of DL-NAM and minimize necroptosis, indicating the role of CTSB in cancer cell inhibition (Figure S29 and S30).

Drug sequestration in lysosome is one of the major problems for drug resistance.<sup>[21]</sup> Encouraged by the fact that our EISA precursors can disrupt the lysosome's integrity, we further investigated whether they can improve drug release from the lysosome. The combination of DL-NAM (62.5 μM) and an anti-cancer chemotherapy drug (DOX, 0.4–10 μM) potentially inhibits U87MG cell viability to 10–13 % of control (Figure 9A), while neither of them alone can inhibit cell viability to lower than 36 %. Notably, the combination of 125 μM DL-NAM and 0.4 μM DOX inhibits 98 % cell viability, suggesting an exceptionally strong synergism. We quantitatively evaluated the synergy effect of DL-NAM and

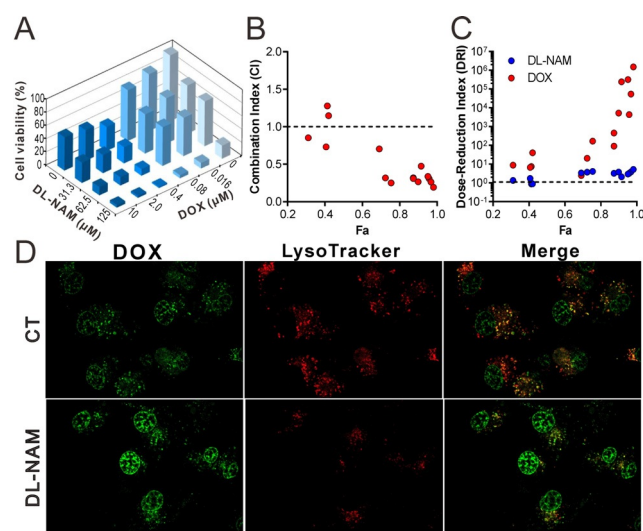


**Figure 9.** A) Cell viability of U87MG cells incubated with DL-NAM and DOX for 24 h. (B) Combination index and C) DRI calculated from (A) according to the Chou–Talalay Method.<sup>[22]</sup> Fa, fraction affected. D) CLSM images of U87MG cells incubated with 10 μM DOX for 1 h and then incubated with 250 μM DL-NAM for another 1 h. Lysosomes were stained by LysoTracker. Scale bar: 20 μM.

DOX by calculating the combination index (CI) that depicts synergism (CI < 1), additive effect (CI = 1) and antagonism (CI > 1).<sup>[22]</sup> CI of most data is small than 1, with 10 out of 15 small than 0.5, indicating a strong synergism effect (Figure 9B). We also calculated plotted dose-reduction index (DRI), which denotes how many folds the dose of each drug may be reduced base on synergism, compared with the dosage of each drug alone.<sup>[22]</sup> According to the DRI diagram, there is a ca. 3 fold and ca. 100 fold dose-reduction for DL-NAM and DOX to achieve 90 % inhibition, respectively (Figure 9C), indicating the synergism effect of DL-NAM and DOX and that DL-NAM can improve the efficiency of DOX toward cancer cells. Strong synergism effect of DL-NAM and DOX was also observed in HeLa cells (Figure S32). In contrast, very weak synergism effect was observed in non-cancer MCF-10A cells (Figure S33). Using CLSM, we detected the distribution of DOX in U87MG cells with or without the treatment of DL-NAM. The results indicate that the distribution of DOX changes significantly after the addition of DL-NAM. Figure 9D shows that the fluorescence from DOX reduce in lysosomes and increased in the nucleus after the cells were treated by DL-NAM (Figure 9D). Meanwhile, impaired staining of lysosome with acidophilic LysoTracker also reveals the disruption of the lysosome by DL-NAM.

## Conclusion

This work reports the programming of functional assemblies in living cells for cancer cell inhibition selectively by the integration of the endocytotic process and enzyme instructed self-assembly. Unlike the emerging concept of biological condensates, the rationally designed artificial assemblies presented in this work provide an easily accessible way to

modulate cell behaviors in a biomimetic strategy. The fully characterized precursors and their bioactivities in living cells illustrate a better understanding of the essential role of serum stability of designed molecules in their bioactivity efficacy. Because of the unique cell death mechanism of our strategy, we also applied it in solving the multidrug resistance of certain drugs by inducing LMP of the lysosome. We predict that the integration of endocytotic process and microenvironment of certain diseases provides a general way to design functional assemblies in living cells and offer an alternative strategy to solve the clinical problem of multidrug resistance.<sup>[23]</sup>

## Acknowledgements

This project was supported by Foundation of Westlake University and Tencent Foundation, the National Natural Science Foundation of China (82022038). We thank Instrumentation and Service Center for Physical Sciences and the CryoEM facility at Westlake University for the assistance work in measurement.

## Conflict of Interest

The authors declare no conflict of interest.

**Keywords:** enzymes · high-order structure · Lysosomal membrane permeabilization · peptides · Self-assembly

- [1] a) E. Busseron, Y. Ruff, E. Moulin, N. Giuseppone, *Nanoscale* **2013**, *5*, 7098–7140; b) B. J. Kim, B. Xu, *Bioconjugate Chem.* **2020**, *31*, 492–500; c) Q. X. Yao, Z. T. Huang, D. D. Liu, J. L. Chen, Y. Gao, *Adv. Mater.* **2019**, *31*, 1804814; d) Z. Q. Q. Feng, T. F. Zhang, H. M. Wang, B. Xu, *Chem. Soc. Rev.* **2017**, *46*, 6470–6479; e) P. P. He, X. D. Li, L. Wang, H. Wang, *Acc. Chem. Res.* **2019**, *52*, 367–378; f) T. Maruyama, W. K. Restu, *Polym. J.* **2020**, *52*, 883–889; g) M. J. Webber, E. A. Appel, E. W. Meijer, R. Langer, *Nat. Mater.* **2016**, *15*, 13–26.
- [2] a) L. Y. Zhao, Q. L. Zou, X. H. Yan, *Bull. Chem. Soc. Jpn.* **2019**, *92*, 70–79; b) G. B. Qi, Y. J. Gao, L. Wang, H. Wang, *Adv. Mater.* **2018**, *30*, 1703444.
- [3] a) B. J. Kim, D. Yang, B. Xu, *Trends Chem.* **2020**, *2*, 71–83; b) M. T. Jeena, L. Palanikumar, E. M. Go, I. Kim, M. G. Kang, S. Lee, S. Park, H. Choi, C. Kim, S. M. Jin, S. C. Bae, H. W. Rhee, E. Lee, S. K. Kwak, J. H. Ryu, *Nat. Commun.* **2017**, *8*, 26; c) J. Gao, J. Zhan, Z. M. Yang, *Adv. Mater.* **2020**, *32*, 1805798.
- [4] a) Y. Hu, H. M. Wang, C. G. Li, J. Y. Liu, B. Xu, W. Di, *Biomater. Sci.* **2020**, *8*, 2007–2017; b) A. N. Shy, J. Li, J. F. Shi, N. Zhou, B. Xu, *J. Drug Targeting* **2020**, *28*, 760–765; c) H. J. He, J. Q. Guo, X. Y. Lin, B. Xu, *Angew. Chem. Int. Ed.* **2020**, *59*, 9330–9334; *Angew. Chem.* **2020**, *132*, 9416–9420; d) H. M. Wang, J. F. Shi, Z. Q. Q. Feng, R. Zhou, S. Y. Wang, A. A. Rodal, B. Xu, *Angew. Chem. Int. Ed.* **2017**, *56*, 16297–16301; *Angew. Chem.* **2017**, *129*, 16515–16519; e) H. M. Wang, Z. Q. Q. Feng, D. D. Wu, K. J. Fritzsche, M. Rigney, J. Zhou, Y. J. Jiang, K. Schmidt-Rohr, B. Xu, *J. Am. Chem. Soc.* **2016**, *138*, 10758–10761.
- [5] R. A. Pires, Y. M. Abul-Haija, D. S. Costa, R. Novoa-Carballal, R. L. Reis, R. V. Ulijn, I. Pashkuleva, *J. Am. Chem. Soc.* **2015**, *137*, 576–579.
- [6] A. Tanaka, Y. Fukuoka, Y. Morimoto, T. Honjo, D. Koda, M. Goto, T. Maruyama, *J. Am. Chem. Soc.* **2015**, *137*, 770–775.
- [7] a) W. Du, X. M. Hu, W. C. Wei, G. L. Liang, *Bioconjugate Chem.* **2018**, *29*, 826–837; b) Y. Cong, L. Ji, Y. J. Gao, F. H. Liu, D. B. Cheng, Z. Y. Hu, Z. Y. Qiao, H. Wang, *Angew. Chem. Int. Ed.* **2019**, *58*, 4632–4637; *Angew. Chem.* **2019**, *131*, 4680–4685; c) G. L. Liang, H. J. Ren, J. H. Rao, *Nat. Chem.* **2010**, *2*, 54–60; d) Z. X. Chen, M. Chen, Y. F. Cheng, T. Kowada, J. H. Xie, X. C. Zheng, J. H. Rao, *Angew. Chem. Int. Ed.* **2020**, *59*, 3272–3279; *Angew. Chem.* **2020**, *132*, 3298–3305; e) J. Zhan, Y. B. Cai, S. S. He, L. Wang, Z. M. Yang, *Angew. Chem. Int. Ed.* **2018**, *57*, 1813–1816; *Angew. Chem.* **2018**, *130*, 1831–1834.
- [8] a) H. M. Wang, Z. Q. Q. Feng, B. Xu, *Angew. Chem. Int. Ed.* **2019**, *58*, 10423–10432; *Angew. Chem.* **2019**, *131*, 10532–10541; b) F. Versluis, J. H. van Esch, R. Eelkema, *Adv. Mater.* **2016**, *28*, 4576–4592.
- [9] a) Z. Q. Q. Feng, H. M. Wang, X. Y. Chen, B. Xu, *J. Am. Chem. Soc.* **2017**, *139*, 15377–15384; b) H. Su, F. Wang, W. Ran, W. Zhang, W. Dai, H. Wang, C. F. Anderson, Z. Wang, C. Zheng, P. Zhang, Y. Li, H. Cui, *Proc. Natl. Acad. Sci. USA* **2020**, *117*, 4518–4526; c) H. M. Wang, Z. Q. Q. Feng, Y. Z. Wang, R. Zhou, Z. M. Yang, B. Xu, *J. Am. Chem. Soc.* **2016**, *138*, 16046–16055.
- [10] A. Küchler, M. Yoshimoto, S. Luginbühl, F. Mavelli, P. Walde, *Nat. Nanotechnol.* **2016**, *11*, 409–420.
- [11] a) B. Turk, *Nat. Rev. Drug Discovery* **2006**, *5*, 785–799; b) M. M. Mohamed, B. F. Sloane, *Nat. Rev. Cancer* **2006**, *6*, 764–775; c) J. C. Widen, M. Tholen, J. J. Yim, A. Antaris, K. M. Casey, S. Rogalla, A. Klaassen, J. Sorger, M. Bogoy, *Nat. Biomed. Eng.* **2021**, *5*, 264–277.
- [12] M. Ma, Y. Kuang, Y. Gao, Y. Zhang, P. Gao, B. Xu, *J. Am. Chem. Soc.* **2010**, *132*, 2719–2728.
- [13] M. K. Shim, J. Park, H. Y. Yoon, S. Lee, W. Um, J. H. Kim, S. W. Kang, J. W. Seo, S. W. Hyun, J. H. Park, Y. Byun, I. C. Kwon, K. Kim, *J. Controlled Release* **2019**, *294*, 376–389.
- [14] a) T. Yamamoto, P. Nair, N. E. Jacobsen, J. Vagner, V. Kulkarni, P. Davis, S. W. Ma, E. Navratilova, H. I. Yamamura, T. W. Vanderah, F. Porreca, J. Lai, V. J. Hruby, *J. Med. Chem.* **2009**, *52*, 5164–5175; b) W. Huang, S. Groothuys, A. Heredia, B. H. M. Kuijpers, F. P. J. T. Rutjes, F. L. van Delft, L. X. Wang, *Chem-BioChem* **2009**, *10*, 1234–1242.
- [15] a) J. Scheike, B. Koksche, *J. Pept. Sci.* **2008**, *14*, 172–172; b) Z. M. Yang, G. L. Liang, M. L. Ma, A. S. Abbah, W. W. Lu, B. Xu, *Chem. Commun.* **2007**, 843–845; c) X. M. Li, Y. Kuang, J. F. Shi, Y. Gao, H. C. Lin, B. Xu, *J. Am. Chem. Soc.* **2011**, *133*, 17513–17518; d) L. S. Birchall, S. Roy, V. Jayawarna, M. Hughes, E. Irvine, G. T. Okorogheye, N. Saudi, E. De Santis, T. Tuttle, A. A. Edwards, R. V. Ulijn, *Chem. Sci.* **2011**, *2*, 1349–1355.
- [16] a) R. W. Chakroun, A. Sneider, C. F. Anderson, F. H. Wang, P. H. Wu, D. Wirtz, H. G. Cui, *Angew. Chem. Int. Ed.* **2020**, *59*, 4434–4442; *Angew. Chem.* **2020**, *132*, 4464–4472; b) J. Li, D. Bullara, X. Du, H. He, S. Sofou, I. G. Kevrekidis, I. R. Epstein, B. Xu, *ACS Nano* **2018**, *12*, 3804–3815.
- [17] a) C. Sinthuvanich, A. S. Veiga, K. Gupta, D. Gaspar, R. Blumenthal, J. P. Schneider, *J. Am. Chem. Soc.* **2012**, *134*, 6210–6217; b) F. Versluis, D. M. van Elsland, S. Mytnyk, D. L. Perrier, F. Trausel, J. M. Poolman, C. Maity, V. A. A. le Sage, S. I. van Kasteren, J. H. van Esch, R. Eelkema, *J. Am. Chem. Soc.* **2016**, *138*, 8670–8673.
- [18] M. Montaser, G. Lalmanach, L. Mach, *Biol. Chem.* **2002**, *383*, 1305–1308.
- [19] X. F. Yao, J. Cao, L. M. Xu, X. C. Sun, J. Kang, G. Yang, L. P. Jiang, C. Y. Geng, C. Z. Gao, L. F. Zhong, Y. F. Ma, *Food Chem. Toxicol.* **2014**, *67*, 96–104.
- [20] a) Y. K. Chan, H. K. Sung, J. W. Jahng, G. H. Kim, M. Han, G. Sweeney, *Mol. Cell. Endocrinol.* **2016**, *430*, 68–76; b) N. M. Templeman, S. Luo, R. Kaletsky, C. Shi, J. Ashraf, W. Keyes, C. T. Murphy, *Curr. Biol.* **2018**, *28*, 753–760, e754.

- [21] a) B. Zhitomirsky, Y. G. Assaraf, *Drug Resist. Updates* **2016**, *24*, 23–33; b) K. J. Gotink, H. J. Broxterman, M. Labots, R. R. de Haas, H. Dekker, R. J. Honeywell, M. A. Rudek, L. V. Beerepoot, R. J. Musters, G. Jansen, A. W. Griffioen, Y. G. Assaraf, R. Pili, G. J. Peters, H. M. W. Verheul, *Clin. Cancer Res.* **2011**, *17*, 7337–7346; c) J. Hraběta, M. Belhajová, H. Šubrtová, M. A. M. Rodrigo, Z. Heger, T. Eckschlager, *Int. J. Mol. Sci.* **2020**, *21*, 4392.
- [22] T. C. Chou, *Cancer Res.* **2010**, *70*, 440–446.
- [23] a) P. Majumder, U. Baxa, S. T. R. Walsh, J. P. Schneider, *Angew. Chem. Int. Ed.* **2018**, *57*, 15040–15044; *Angew. Chem.* **2018**, *130*, 15260–15264; b) J. G. Huang, J. C. Li, Y. Lyu, Q. Q. Miao, K. Pu, *Nat. Mater.* **2019**, *18*, 1133–1143; c) J. C. Li, Y. Luo, K. Y. Pu, *Angew. Chem. Int. Ed.* **2021**, *60*, 12682–12705; *Angew. Chem.* **2021**, *133*, 12792–12815.

Manuscript received: March 10, 2021  
Revised manuscript received: May 28, 2021  
Accepted manuscript online: June 29, 2021  
Version of record online: July 26, 2021